Published in final edited form as:
J Neurosci Methods. 2014 April 30; 227: 10–17. doi:10.1016/j.jneumeth.2014.01.035.

High resolution MRI anatomy of the cat brain at 3 Tesla

Heather L. Gray-Edwards[1], **Nouha Salibi**[2], **Eleanor M. Josephson**[3], **Judith A. Hudson**[4], **Nancy R. Cox**[1], **Ashley N. Randle**[1], **Victoria J. McCurdy**[1,3], **Allison M. Bradbury**[1,3], **Diane U. Wilson**[1], **Ronald J. Beyers**[6], **Thomas S. Denney**[5,6], and **Douglas R. Martin**[1,3]

[1]Scott-Ritchey Research Center, Auburn University, Auburn AL, United States

[2]MR R&D Siemens Healthcare, Malvern PA, United States

[3]Department of Anatomy, Physiology and Pharmacology, Auburn University, Auburn, AL, United States

[4]Department of Clinical Sciences, College of Veterinary Medicine, Auburn University, Auburn AL, United States

[5]Department of Electrical and Computer Engineering, Auburn University, Auburn AL, United States

[6]Auburn University MRI Research Center, Auburn, Al United States

Abstract

Background—Feline models of neurologic diseases, such as lysosomal storage diseases, leukodystrophies, Parkinson's disease, stroke and NeuroAIDS, accurately recreate many aspects of human disease allowing for comparative study of neuropathology and the testing of novel therapeutics. Here we describe in vivo visualization of fine structures within the feline brain that were previously only visible post mortem.

New Method—3 Tesla MR images were acquired using T1-weighted (T1w) 3D magnetization-prepared rapid gradient echo (MPRAGE) sequence (0.4mm isotropic resolution) and T2-weighted (T2w) turbo spin echo (TSE) images ($0.3\times0.3\times1$ mm^3 resolution). Anatomic structures were identified based on feline and canine histology.

Results—T2w high resolution MR images with detailed structural identification are provided in transverse, sagittal and dorsal planes. T1w MR images are provided electronically in three dimensions for unrestricted spatial evaluation.

Comparison with Existing Methods—Many areas of the feline brain previously unresolvable on MRI are clearly visible in three orientations, including the dentate, interpositus and fastigial cerebellar nuclei, cranial nerves, lateral geniculate nucleus, optic radiation, cochlea, caudal colliculus, temporal lobe, precuneus, spinocerebellar tract, vestibular nuclei, reticular formation,

Corresponding Author: Heather L. Gray Edwards, Scott Ritchey Research Center, College of Veterinary Medicine, 1265 H.C. Morgan Dr., Auburn University, Al 36849-5525, +01 (334)844-5951, +01 (334)844-5950 (fax), grayhea@auburn.edu.

pyramids and rostral and middle cerebral arteries. Additionally, the feline brain is represented in 3 dimensions for the first time.

Conclusions—These data establish normal appearance of detailed anatomical structures of the feline brain, which provide reference when evaluating neurologic disease or testing efficacy of novel therapeutics in animal models.

Keywords

Cat; MRI; Brain; Central Nervous System; Translational; Animal Model

Introduction

Advances in the study and treatment of neurologic disease have frequently depended upon animal modeling. While murine models have been vital, they do not always reproduce human anatomy or disease faithfully (Phaneuf et al., 1996, Ohshima et al., 1997, Casal et al., 2006). Also, mouse brain size (>1,000 times smaller than humans) and complexity necessitate testing of therapeutics in larger animals before initiation of clinical trials. Large animal modeling is a logical intermediate step between murine models and humans because of increasing similarity in neuropathology (Baker et al., 1971, Cork et al., 1978, Aye et al., 1998, Podell et al., 2000), immunology (Hein et al., 2003, Costa et al., 2012, Meurens et al., 2012) and biodistribution challenges (Vite et al., 2003). Large animal models also facilitate longitudinal studies due to their increased lifespan. For example the dog is a valuable model for neurologic diseases such as glioblastoma (Candolfi et al., 2007), and another widely investigated non-rodent species is the cat. Feline models of neurologic disease are numerous and include Parkinson's disease (Schneider et al., 1986), NeuroAIDS (Abramo et al., 1995, Bendinelli et al., 1995), stroke (Toyota et al., 2002, Lee et al., 2004, Strong et al., 2007), trauma (Hilton et al., 1993, Khan et al., 1999) and lysosomal storage diseases such as the gangliosidoses (Baker et al., 1971, Cork et al., 1977, Martin et al., 2004, Bradbury et al., 2009, Bradbury et al., 2013), mucopolysaccharidoses (Haskins et al., 1979, Haskins et al., 1981, Gitzelmann et al., 1994), alpha-mannosidosis (Burditt et al., 1980), Krabbe disease (Suzuki, 1985) and Neiman-Pick Type C (Lowenthal et al., 1990). Feline models have provided invaluable information about human neurologic diseases, and novel therapeutics have been tested in cat models for eventual clinical use (Vite et al., 2005, Vite et al., 2011, Bradbury et al., 2013, Bucher et al., 2013).

The value and expense of large animal models, and longitudinal studies therein, make non-invasive methods to evaluate intracranial disease increasingly important. MRI, the modality of choice for non-invasive brain imaging, has been used to evaluate disease progression in feline models of Parkinson's disease (Podell et al., 2003), alpha-mannosidosis (Vite et al., 2001, Vite et al., 2008), hydrocephalus (Eskandari et al., 2011), cerebral edema (Fatouros et al., 1999), and gangliosidosis (Kroll et al., 1995, Hasegawa et al., 2007). Also, MRI has been used to measure therapeutic success of AAV-gene therapy in feline GM1 and GM2 gangliosidosis (Bradbury, 2013, Johnson, 2013, McCurdy, 2013) and feline alpha-mannosidosis (Vite et al., 2005). As these therapies approach human clinical trials, in-depth analysis of changes within specific brain structures will be vital for understanding effects of therapy. Currently, the feline brain MRI anatomy is available at reduced resolution from

lower field-strength MRI (1.5 Tesla) (Mogicato et al., 2012), but advances in MRI technology have led to high-field strength MRI in neurologic disease research. MRI at ~3 Tesla (3T) is the highest field strength currently approved by the Food and Drug Administration (FDA) for human patients and images collected at this field strength provide pronounced improvements in image clarity and detail in feline models. Here we show for the first time high resolution (3T) T2 weighted (T2w) MRI images of the feline brain, including anatomical structure identification in the transverse, sagittal and dorsal views. We also include T1-weighted (T1w) imaging in three dimensions for complete spatial evaluation.

Materials and Methods

The adult cat brain clinical anatomy was evaluated in 6 doligocephalic healthy cats of various ages: 2 male intact domestic long-haired cats (DLH), both 13 months of age (littermates) and 5 female intact domestic short-haired or DLH cats ages 6, 24, 31 and 47 months. The cats in this study are from experimental breeding colonies which have been meticulously maintained for >40 years; therefore, complete medical history was known and recorded. In addition, full physical and neurological examinations were performed on all cats at the time of MRI to ensure the absence of underlying systemic or neurologic disease. Cats were anesthetized using an initial intramuscular dose of dexmedetomidine (0.04mg/kg Pfizer, New York, NY) and ketamine (10mg/kg Fort Dodge, Overland Park, KS), and anesthesia was maintained using isoflurane (Henry Schein, Dublin, OH) at 0.25–2% with 1L/min 100% oxygen to desired effect. Cats were placed in sternal recumbency for MRI scanning. Cats were humanely euthanized by intravenous pentobarbital overdose (100 mg/kg Euthosol, Virbac, Fort Worth, TX) after a pre-anesthetic dose of dexmedetomidine (0.04mg/kg) and ketamine (10–20 mg/kg) which complies with the American Veterinary Medical Association Guidelines for Euthanasia. The brain was then perfused through the carotid artery with cold 0.9% sodium chloride, removed from the cranial vault and cut into nine blocks (6 mm each) along the transverse plane. Gross sections from cats were closely evaluated for consistency, and gross images from a representative brain are shown. All experimental procedures were approved by the Auburn University Institutional Animal Care and Use Committee and followed guidelines set forth in the National Institutes of Health Guide for the Care and Use of Laboratory Animals.

All MRI scans were performed on a 3 Tesla MAGNETOM Verio scanner (Siemens Healthcare, Erlangen, Germany) using an 8 channel phased array human wrist coil (Invivo Corp, Gainesville, FL, USA). Anatomical images were acquired using 3D T1w magnetization-prepared rapid acquisition gradient echo (MPRAGE) with 0.4mm isotropic resolution, TR/TI/TE of 1900/900/3.3 ms, flip angle of 9 degrees, bandwith (BW) of 170 Hz/pixel, and five averages. This was supplemented with 2D transverse and dorsal T2w turbo spin echo (TSE) images with $0.3\times0.3\times1mm^3$ resolution, TR/TE of 4630/107 ms, echo train length of 9, BW of 243 Hz/pixel, and six averages. MRI slices were oriented as follows: transverse sections perpendicular to ventral aspect of brain, sagittal parallel with the interthalamic adhesion, and dorsal parallel to ventral aspect of the brain.

Images were reviewed using EFilm 3.2 software (Merge Healthcare, Chicago, IL, USA). Anatomic structures were identified using a previously published MRI-based atlas

(Mogicato et al., 2012) and the feline (Bleier et al., 1961, Snider et al., 1970) and canine (Singer et al., 1962, Buxton et al., 1986) histologic atlases. Anatomical structure nomenclature follows the format of the Illustrated Veterinary Anatomical Nomenclature (Schaller et al., 2007) and Nomina Anatomica Verterinaria (I.C.V.G.A.N. et al., 2005). Veterinary anatomical nomenclature differs from human and, because the information contained herein is intended for researchers in human medicine as well, the conversion of directional terms is as follows (human=veterinary): coronal=dorsal, axial=transverse and sagittal is consistent in both nomenclatures (Dyce et al., 2009).

Results

Transverse T2w images include nine sections starting at the frontal cortex and extending through the striatum, thalamus, occipital cortex/midbrain and cerebellum/brainstem. These image slices correspond to reference lines A–I present on the sagittal and dorsal view localizer images (Figure 1a, b and c). T2w dorsal images include eight sections starting with the dorsal portion of the gyri and extending ventrally with clear identification of areas within the striatum, thalamus, cerebellar folia, hypothalamus, cerebellar nuclei, midbrain and brainstem, with the deepest images clearly showing the optic and trigeminal nerves as well as pituitary gland (Figure 2). These images correspond with reference lines A–H on the sagittal and transverse localizer images (Figure 3). T2w sagittal images include four sections of one hemisphere (Figure 3) starting at midline and extending laterally. Images correspond with reference lines AD on the transverse and dorsal localizer images. Individual structures are identified in three dimensions and denoted by numbers, which correlate with the structures listed in the image key. An index of structures arranged alphabetically is also provided.

T2w MR images show excellent resolution and contrast between gray/white matter and ventricular structures. Intensities of general brain components are appropriate and clearly visualized, from greatest to least: CSF > gray matter > white matter. Surface gyri and sulci are easily distinguished on all images as well as deeper structures within the frontal cortex, internal capsule, caudate, striatum, thalamus, midbrain, cerebellum and brainstem. Several areas previously reported to be unresolvable on MRI, such as the dentate, interpositus and fastigial cerebellar nuclei and vestibular nuclei (Mogicato et al., 2012), are clearly identified (Figures 1c, 2 and 3). The visual pathway is apparent starting from the optic nerve through the chiasm and tract to the lateral geniculate nucleus and optic radiation (Figure 1b, 2, 3). Constituents of the auditory pathway (the cochlea, caudal colliculus, medial geniculate nucleus and temporal lobe) are clearly shown (Figure 1b, 2, 3). Areas of the motor pathways are also visualized, including the precuneus, spinocerebellar tract, vestibular nuclei, reticular formation, pyramids and internal capsule (Figure 1b, 2, 3). The vasculature of the feline brain is identified on MR images with clear resolution of the rostral and middle cerebral arteries in three planes (Figure 1b, 2, 3).

The feline MRI atlas is enriched further by three-dimensional, T1w MPRAGE images. As typical with T1-weighting, the MPRAGE sequence exhibits hyperintense white matter as compared to gray matter and hypointense CSF to both cortical intensities. These images are interactive so that the reader will able to zoom, rotate, as well as download the 3D

reconstruction. Resolution of these T1w images is comparable to that of the T2w images (Figures 1–3) with visualization of all gyri and sulci as well as deeper cortical and cerebellar structures previously identified in great detail. This supplementary online figure facilitates comparison of locations of specific structures and evaluates their exact location in the other planes.

Discussion

Higher magnetic field strengths (3T) have been used frequently in both the research and clinical setting since their FDA approval in 2000. Increased magnetic field results in improved signal to noise ratio (SNR), to approximately twice that of 1.5T (Takahashi et al., 2003). This increase of SNR translates to improved spatial and contrast resolution resulting in superior visualization of small brain lesions in various neurological conditions (Duewell et al., 1996, Knake et al., 2005, Alvarez-Linera, 2008, Bote et al., 2008, Woermann et al., 2009). Detailed anatomical structures, such as, the hippocampus are clearly resolved at 3T and this advance in technology has led to improved diagnosis of various forms of epilepsy (Knake et al., 2005, Sawaishi et al., 2005, Woermann et al., 2009) multiple sclerosis (Wattjes et al., 2006), metastatic disease (Ba-Ssalamah et al., 2003) and cerebral ischemia (Kuhl et al., 2005). The detail of the visual and auditory pathways provided in these images may lend insight to the etiology in blindness and hearing loss in animal models. For example, 3T assessment of the integrity of the lateral lemniscus and acoustic radiation can lead to diagnosis of sensorineural hearing loss; and tinnitus can also be diagnosed using MRI modalities (Smits et al., 2007, Johansen-Berg et al., 2009). Additionally, high field MRI can detect optic neuritis, which is often the first diagnostic sign in multiple sclerosis (Vinogradov et al., 2005).

The cat model offers many advantages in the study of neurological diseases. Organization of the cat brain is similar to that of humans, with analogous regions of function and physiology, and the cat brain provides certain research advantages over the mouse brain (Bleier, 1961, Berman, 1968, Snider, 1970, Berman, 1982, Vite et al., 2005). Several naturally occurring cat models of neurologic disorders are currently used in translational research to test therapeutics (Ellinwood et al., 2004, Vite et al., 2005, Bradbury et al., 2013). It has been reported that the increased complexity and large size of the cat brain highlights regional effects of therapy that would likely be experienced in humans (Vite et al., 2005). As the use of high field strength MRI expands in translational research, the ability to identify brain structures detailed herein will aid correlation with human disease and assessment of therapeutic success.

Image Key

#) English name – *Latin Name* (Locations identified)

1. Olfactory tract – *Tractus olfactorius* (Fig 1a:A′, Fig 2:C′, E′)
2. Presylvian sulcus – *Sulcus presylvius* (Fig 1a:A′)
3. Cruciate sulcus – *Sulcus cruciatus* (Fig 1a:A′, Fig 2:A′, Fig 3:A′,)

4. Frontal gyrus – *Gyrus frontalis* (Fig 1a:A′, Fig 2:B′, C′, Fig 3:B′)
5. Rectal gyrus – *Gyrus rectus* (Fig 1a:A′)
6. Precuneus (Fig 1a:B′, Fig 2:A′, Fig 3:A′)
7. Longitudinal fissure – *Fissure longitudinalis* (Fig 1a:B′, Fig 2:A′)
8. Rostral suprasylvian gyrus – *Gyrus suprasylvius rostralis* (Fig 1a:B′)
9. Lateral ventricle – *Ventriculus lateralis* (Fig 1a:B′, Fig 1b:C′, D′, E′, Fig 2:B′, D′, Fig 3:D′)
10. Rhinal fissure – *Fissura rhinalis* (Fig 1a:B′)
11. *Corpus callosum* (Fig 1b:C′, E′)
12. Cingulate gyrus – *Gyrus cinguli* (Fig 1a:B′, Fig 1b:C′, D′E′F′, Fig 2:A′, Fig 3:A′B′
13. Caudate nucleus – *Nucleus caudatus* (Fig 1b:C′, Fig 2:B′, C′, D′, E′, Fig 3:B′)
14. *Putamen* (Fig 1b:C′, Fig 2:E′)
15. Accumbens nucleus – *Nucleus accumbens* (Fig 1b:C′)
16. Optic nerve –*Nervus opticus* (Fig 1b:C′, Fig 2:F′, Fig 3:B′)
17. *Corona radiata* (Fig 1b:C′, Fig 3:D′)
18. Coronal sulcus – *Sulcus coronalis* (Fig 1b:C′)
19. Post-cruciate sulcus – *Sulcus postcruciatus* (Fig 1b:C′)
20. Rostral ectosylvian gyrus – *Gyrus ectosylvius rostralis* (Fig 1b:C′)
21. Optic chiasm – *Chiasma opticum* (Fig 1b:D′, Fig 2:F′, Fig 3:A′)
22. Mammillary body – *Corpus mamillare* (Fig 1b:D′, Fig 3:A′)
23. *Amygdala* (Fig 1b:D′, Fig 2:F′, Fig 3:D′)
24. *Thalamus* (Fig 1b:D′E′, Fig 2:C′, Fig 3:B′, C′)
25. Endopeduncular nucleus – *Nucleus endopenduncularis* (Fig 1b:D′)
26. *Hypothalamus* (Fig 1b:D′, Fig 2:F′, Fig 3:B′C′)
27. *Stria medularis thalami* (Fig 1b:D′)
28. Choroid artery (Fig 1b:D′)
29. *Hippocampus* (Fig 1b:D′, E′F′, Fig 2:B′, Fig 3:A′, B′C′)
30. Corpus callosum radiation – *Radiatio corpus callosi* (Fig 1b:D′)
31. Suprasylvian gyrus – *Gyrus suprasylvius* (Fig 1b:D′F′, Fig:2A′, Fig 3:C′, D′)
32. Ectosylvian gyrus – *Gyrus ectosylvius* (Fig 1b:D′, Fig 2:A′, Fig 3:D′)
33. Suprasplenial gyrus- *Gyrus suprasplenialis* (Fig 1b:D′, E′, F′, Fig 3:B′)
34. Splenial gyrus – *Gyrus splenialis* (Fig 1b:D′, E′, F′, Fig 2:A′, Fig 3:A′)

35. Temporal lobe - *Lobus temporalis* (Fig 1b:D′)
36. Mesencephalic aqueduct –*Aqueductus mesencephali* (Fig 1b:E′, F′, Fig 2:E′, Fig 3:A′)
37. Lateral geniculate nucleus – *Nucleus geniculatus lateralis* (Fig 1b:E′, Fig 2:C′D′)
38. Optic radiation – *Radiatio optica* (Fig 1b:E′, F′)
39. Rostral sigmoidean gyrus – *Gyrus sigmoideus rostralis* (Fig 2:A′)
40. Parahippocampal gyrus – *Gyrus parahippocampalis* (Fig 1b:E′)
41. Lateral sulcus - *Sulcus lateralis* (Fig 1b:D′, F′)
42. Suprasylvian sulcus – *Sulcus suprasylvius* (Fig 1b:D′, F′, Fig 2:A′)
43. Choroid plexus– *Tela choroidea* (Fig 1b:E′, Fig 2:B′)
44. Pulivinar nucleus – *Nucleus pulvinaris* (Fig 1b:E′)
45. Medial geniculate nucleus – *Nucleus geniculatus medialis* (Fig 1b:E′, Fig 2:E′)
46. *Substantia nigra* (Fig 1b:E′, Fig 2F′)
47. Periaqueductal gray- *Substantia grisea centralis* (Fig 1b:F′)
48. Rostral colliculus – *Colliculus rostralis* (Fig 1b:F′, Fig 2:C′, D′, E′, Fig 3:B′)
49. *Pons* (Fig 1b:F′, Fig 2:G′, H′, Fig 3:A′, B ′, C′)
50. Middle cerebellar peduncle – *Pedunculus cerebellaris medius* (Fig 1b:F′)
51. Mesencephalon (Fig 1b:F′, Fig 3:A′)
52. Splenial sulcus - *Sulcus splenialis* (Fig 1b:E′F′, Fig 3:A′)
53. Occipital cortex – *Cortex occipitalis* (Fig 1b:F′, Fig 1c:G′, Fig 3:B′)
54. Caudal colliculus – *Colliculus caudalis* (Fig 1b:F′, Fig 2:D′, E′, Fig 3:B′)
55. Rostral colliculus commissure – *Commissura colliculus rostralis* (Fig 1b:F′, Fig 2:D′)
56. *Flocculus* (Fig 2:F′)
57. Caudal colliculus commissure – *Commissura colliculus caudalis* (Fig 2:D′)
58. *Lingula* (Fig 1c:G′, Fig 2:F′, Fig 3:A′)
59. Cochlear nucleus – *Nucleus cochlearis* (Fig 1c:G′)
60. Pyramids – *Pyramis* (Fig 1c:G′, I′, Fig 3:B′)
61. Medial longitudinal fasciculus – *Faciculus longitudinalis medialis* (Fig 1c:G′)
62. Vestibular nucleus – *Nucleus vestibularis* (Fig 1c:G′, H′)
63. Caudal cerebellar peduncle – *Pedunculus cerebellaris caudalis* (Fig 1c:G′)

64. Dorsal nucleus of the trapezoid body – *Nucleus dorsalis corporis trapezoidei* (Fig 1c:G′)
65. *Medulla oblongata* (Fig 1c:G′, Fig 3:A′)
66. Rostral cerebellum – *Lobulus centralis* (Fig 1c:G′, Fig 2:C′, E′)
67. *Paraflocculus* (Fig 1c:G′)
68. Fastigial nucleus – *Nucleus fastigii* (Fig 1c:H′ Fig 2:E′)
69. Interpositus nucleus – *Nucleus interpositus* (Fig 1c:H′, Fig 2:E′, F′)
70. Dentate nucleus – *Nucleus dentatus* (Fig 1c:H′, Fig 2:E′, F′)
71. *Nodulus* (Fig 1c:H′, Fig 3:A′)
72. Ramus of suprasylvian gyrus (Fig 2:A′)
73. Olivary nucleus – *Nucleus olivaris* (Fig 1c:H′)
74. Reticular formation – *Formatio reticularis* (Fig 1c:H′, I′, Fig 3:B′)
75. Optic tract – *Tractus opticus* (Fig 2:F′)
76. Spinocerebellar tract – *Tractus spinocerebellaris* (Fig 1c:H′, I′)
77. *Vermis* (Fig 1c:I′, Fig 2C′, D′)
78. Fourth ventricle – *Ventricularis quartus* (Fig 1c:H′, I′, Fig 3:A′)
79. Spinal tract of trigeminal nerve – *Tractus spinalis n. trigemini* (Fig 1c:I′)
80. Paramedian lobule – *Lobulus paramedianus* (Fig 1c:I′, Fig 2:F′)
81. Ansiform lobule – *Lobulus ansiformis* (Fig 1c:I′, Fig 2:F′)
82. Internal capsule – *Capsula interna* (Fig 1b:C′, Fig 2:B′, C′, D′, E′)
83. Third ventricle – ventral part – *Ventricularis tertius* (Fig 1b:D, Fig 2:E′)
84. Third ventricle – dorsal part – *Ventricularis tertius* (Fig 1b:D′, Fig 3:A′)
85. *Crus cerebri* (Fig 1b:E′)
86. Ventral part of hippocampus (Fig 1b:D′, E′, Fig 2:E′F′, Fig 3:D′)
87. Olfactory bulb – *Bulbus olfactorius* (Fig 2:D′E′, Fig 3:A′)
88. Parolfactory gyrus- *Gyrus parolfactorius* (Fig 2:E′, Fig 3:A′)
89. Post-lateral gyrus (Fig 2:A′)
90. Post-cruciate gyrus –*gyrus postcruciatus* (Fig 2:A′, Fig 3:B′)
91. Post-lateral sulcus (Fig 2:A′)
92. Pineal gland – *Glandula pinealis* (Fig 2:C′)
93. Splenium of corpus callosum – *Splenium corporis callosi* (Fig 2:B′ Fig 3:A′)
94. Genu of corpus callosum – *Genu corporis callosi* (Fig 2:B′, Fig 3:A′)

95. *Cerebellum* (Fig 2:B′)

96. Interthalamic adhesion – *Adhesio interthalami* (Fig 2:C′, D′, E′ Fig 3:A′)

97. Cerebellar hemisphere – *Hemispherium cerebelli* (Fig 2:C′, D′, Fig 3D′)

98. Pyriform lobe – *Lobus piriformis* (Fig 2:F′)

99. CN V - Trigeminal nerve – *Nervus trigeminus* (Fig 2:G′)

100. *Uvula* (Fig 2:E′, F′, Fig 3:A′)

101. Middle cerebral artery (Fig 2:B′, F′)

102. Pituitary – *Hypophysis* (Fig 2:G′, Fig 3:A′)

103. Central canal - *Canalis centralis* (Fig 2:H′, Fig 3:A′)

104. Septum – *Septum telencephali (cellulare)* (Fig 2:C′, Fig 3A′)

105. *Fornix* (Fig 3:A′)

106. Tectum of mesencephalon – *Tectum mesencephali* (Fig 3:A′)

107. Lateral lemniscus – *Lemniscus lateralis* (Fig 2:F′)

108. Medullary velum – *Velum medullare* (Fig 3:A′)

109. Rostral commissure - *Commissura rostralis* (Fig 2:E′, Fig 3:A′)

110. Spinal cord – *Medulla spinalis* (Fig 3:A′)

111. Primary fissure - *Fissura prima* (Fig 3:A′)

112. Rostral cerebral artery (Fig 2:D′, F′ Fig 3:B′)

113. *Cochlea* (Fig 3:D′)

114. Cerebellar white matter – (Fig 3:A′, B′)

115. Oculomotor nerve – *Nervus oculomotorius* (Fig 3:B′)

116. *Pes mesencephali* (Fig 3:B′)

117. Trapezoid body – *Corpus trapezoideum* (Fig 3:B′)

118. Cerebellar peduncles (Fig 3:C′)

119. Marginal gyrus – *Gyrus Marinalis* (Fig 3:A′)

Index

English name – *Latin Name* # (Locations identified)

Accumbens nucleus – *Nucleus accumbens* **#15** (Fig 1b:C′)

Amygdala **#23** (Fig 1b:D′, Fig 2:F′, Fig 3:D′)

Ansiform lobule – *Lobulus ansiformis* **#81** (Fig 1c:I′, Fig 2:F′)

Caudal cerebellar peduncle – *Pedunculus cerebellaris caudalis* **#63** (Fig 1c:G′)

Caudal colliculus – *Colliculus caudalis* **#54** (Fig 1b:F′, Fig 2:D′, E′, Fig 3:B′)

Caudal colliculus commissure – *Commissura colliculus caudalis* **#57** (Fig 2:D′)

Caudate nucleus – *Nucleus caudatus* **#13** (Fig 1b:C′, Fig 2:B′, C′, D′, E′, Fig 3:B′)

Central canal - *Canalis centralis* **#103** (Fig 2:H′, Fig 3:A′)

Cerebellar hemisphere – *Hemispherium cerebelli* **#97** (Fig 2:C′, D′, Fig 3D′)

Cerebellar peduncles **#118** (Fig 3:C′)

Cerebellar white matter **#114** (Fig 3:A′, B′)

Cerebellum **#95** (Fig 2:B′)

Choroid artery **#28** (Fig 1b:D′)

Choroid plexus– *Tela choroidea* **#43** (Fig 1b:E′, Fig 2:B′)

Cingulate gyrus – *Gyrus cinguli* **#12** (Fig 1a:B′, Fig 1b:C′, D′, E′, F′, Fig 2:A′, Fig 3:A′B′

CN V - Trigeminal nerve – *Nervus trigeminus* **#99** (Fig 2:G′)

Cochlea **#113** (Fig 3:D′)

Cochlear nucleus – *Nucleus cochlearis* **#59** (Fig 1c:G′)

Corona radiata **#17** (Fig 1b:C′, Fig 3:D′)

Coronal sulcus – *Sulcus coronalis* **#18** (Fig 1b:C′)

Corpus callosum **#11** (Fig 1b:C′, E′)

Corpus callosum radiation – *Radiatio corpus callosi* **#30** (Fig 1b:D′)

Cruciate sulcus – *Sulcus cruciatus* ***#3*** (Fig 1a:A′, Fig 2:A′, Fig 3:A′)

Crus cerebri **#85** (Fig 1b:E′)

Dentate nucleus – *Nucleus dentatus* **#70** (Fig 1c:H′, Fig 2:E′, F′)

Dorsal nucleus of the trapezoid body – *Nucleus dorsalis corporis trapezoidei* **#64** (Fig 1c:G′)

Ectosylvian gyrus – *Gyrus ectosylvius* **#32** (Fig 1b:D′, Fig 2:A′, Fig 3:D′)

Endopeduncular nucleus – *Nucleus endopenduncularis* **#25** (Fig 1b:D′)

Fastigial nucleus – *Nucleus fastigii* **#68** (Fig 1c:H′ Fig 2:E′)

Flocculus **#56** (Fig 2:F′)

Fornix **#105** (Fig 3:A′)

Fourth ventricle – *Ventricularis quartus* **#78** (Fig 1c:H′, I′, Fig 3:A′)

Frontal gyrus – *Gyrus frontalis* **#4** (Fig 1a:A′, Fig 2:B′, C′, Fig 3:B′)

Genu of corpus callosum – *Genu corporis callosi* **#94** (Fig 2:B′, Fig 3:A′)

Hippocampus **#29** (Fig 1b:D′, E′F′, Fig 2:B′, Fig 3:A′, B′C′)

Hypothalamus **#26** (Fig 1b:D′, Fig 2:F′, Fig 3:B′C′)

Internal capsule – *Capsula interna* **#82** (Fig 1b:C′, Fig 2:B′, C′, D′, E′)

Interpositus nucleus – *Nucleus interpositus* **#69** (Fig 1c:H′, Fig 2:E′, F′)

Interthalamic adhesion – *Adhesio interthalami* **#96** (Fig 2:C′, D′, E′ Fig 3:A′)

Lateral geniculate nucleus – *Nucleus geniculatus lateralis* **#37** (Fig 1b:E′, Fig 2:C′D′)

Lateral lemniscus – *Lemniscus lateralis* **#107** (Fig 2:F′)

Lateral sulcus - *Sulcus lateralis* **#41** (Fig 1b:D′, F′)

Lateral ventricle – *Ventriculus lateralis* **#9** (Fig 1a:B′, Fig 1b:C′, D′, E′, Fig 2:B′, D′, Fig 3:D′)

Lingula **#58** (Fig 1c:G′, Fig 2:F′, Fig 3:A′)

Longitudinal fissure – *Fissure longitudinalis* **#7** (Fig 1a:B′, Fig 2:A′)

Mammillary body – *Corpus mamillare* **#22** (Fig 1b:D′, Fig 3:A′)

Marginal gyrus – *Gyrus Marinalis* **#119** (Fig 3:A′)

Medial geniculate nucleus – *Nucleus geniculatus medialis* **#45** (Fig 1b:E′, Fig 2:E′)

Medial longitudinal fasciculus – *Faciculus longitudinalis medialis* **#61** (Fig 1c:G′)

Medulla oblongata **#65** (Fig 1c:G′, Fig 3:A′)

Medullary velum – *Velum medullare* **#108** (Fig 3:A′)

Mesencephalic aqueduct –*Aqueductus mesencephali* **#36**(Fig 1b:E′, F′, Fig 2:E′, Fig 3:A′)

Mesencephalon **#51** (Fig 1b:F′, Fig 3:A′)

Middle cerebellar peduncle – *Pedunculus cerebellaris medius* **#50** (Fig 1b:F′)

Middle cerebral artery **#101** (Fig 2:B′, F′)

Nodulus **#71** (Fig 1c:H′, Fig 3:A′)

Occipital cortex – *Cortex occipitalis* **#53** (Fig 1b:F′, Fig 1c:G′, Fig 3:B′)

Oculomotor nerve – *Nervus oculomotorius* **#115** (Fig 3:B′)

Olfactory bulb – *Bulbus olfactorius* **#87** (Fig 2:D′E′, Fig 3:A′)

Olfactory tract – *Tractus olfactorius* **#1** (Fig 1a:A′, Fig 2:C′, E′)

Olivary nucleus – *Nucleus olivaris* **#73** (Fig 1c:H′)

Optic chiasm – *Chiasma opticum* **#21** (Fig 1b:D′, Fig 2:F′, Fig 3:A′)

Optic nerve –*Nervus opticus* **#16** (Fig 1b:C′, Fig 2:F′, Fig 3:B′)

Optic radiation – *Radiatio optica* **#38** (Fig 1b:E′, F′)

Optic tract – *Tractus opticus* **#75** (Fig 2:F′)

Paraflocculus **#67** (Fig 1c:G′)

Parahippocampal gyrus – *Gyrus parahippocampalis* **#40** (Fig 1b:E′)

Paramedian lobule – *Lobulus paramedianus* **#80** (Fig 1c:I′, Fig 2:F′)

Parolfactory gyrus- *Gyrus parolfactorius* **#88** (Fig 2:E′, Fig 3:A′)

Periaqueductal gray- *Substantia grisea centralis* **#47** (Fig 1b:F′)

Pes mesencephali **#116** (Fig 3:B′)

Pineal gland – *Glandula pinealis* **#92** (Fig 2:C′)

Pituitary – *Hypophysis* **#102** (Fig 2:G′, Fig 3:A′)

Pons **#49** (Fig 1b:F′, Fig 2:G′, H′, Fig 3:A′, B′, C′)

Post-cruciate gyrus –*gyrus postcruciatus* **#90** (Fig 2:A′, Fig 3:B′)

Post-cruciate sulcus – *Sulcus postcruciatus* **#19** (Fig 1b:C′)

Post-lateral gyrus **#89** (Fig 2:A′)

Post-lateral sulcus **#91** (Fig 2:A′)

Precuneus **#6** (Fig 1a:B′, Fig 2:A′, Fig 3:A′)

Presylvian sulcus – *Sulcus presylvius* **#2** (Fig 1a:A′)

Primary fissure - *Fissura prima* **#111** (Fig 3:A′)

Pulivinar nucleus – *Nucleus pulvinaris* **#44** (Fig 1b:E′)

Putamen **#14** (Fig 1b:C′, Fig 2:E′)

Pyramids – *Pyramis* **#60** (Fig 1c:G′, I′, Fig 3:B′)

Pyriform lobe – *Lobus piriformis* **#98** (Fig 2:F′)

Ramus of suprasylvian gyrus **#72** (Fig 2:A′)

Rectal gyrus – *Gyrus rectus* **#5** (Fig 1a:A′)

Reticular formation – *Formatio reticularis***#74** (Fig 1c:H′, I′, Fig 3:B′)

Rhinal fissure – *Fissura rhinalis* **#10** (Fig 1a:B′)

Rostral cerebellum – *Lobulus centralis* **#66** (Fig 1c:G′, Fig 2:C′, E′)

Rostral cerebral artery **#112** (Fig 2:D′, F′ Fig 3:B′)

Rostral colliculus – *Colliculus rostralis* **#48** (Fig 1b:F′, Fig 2:C′, D′, E′, Fig 3:B′)

Rostral colliculus commissure – *Commissura colliculus rostralis* **#55** (Fig 1b:F′, Fig 2:D′)

Rostral commissure - *Commissura rostralis* **#109** (Fig 2:E′, Fig 3:A′)

Rostral ectosylvian gyrus – *Gyrus ectosylvius rostralis* **#20** (Fig 1b:C′)

Rostral sigmoidean gyrus – *Gyrus sigmoideus rostralis* **#39** (Fig 2:A′)

Rostral suprasylvian gyrus – *Gyrus suprasylvius rostralis* **#8** (Fig 1a:B′)

Septum – *Septum telencephali (cellulare)* **#104** (Fig 2:C′, Fig 3A′)

Spinal cord – *Medulla spinalis* **#110** (Fig 3:A′)

Spinal tract of trigeminal nerve – *Tractus spinalis n. trigemini* **#79** (Fig 1c:I′)

Spinocerebellar tract – *Tractus spinocerebellaris* **#76** (Fig 1c:H′, I′)

Splenial gyrus – *Gyrus splenialis* **#34** (Fig 1b:D′, E′, F′, Fig 2:A′, Fig 3:A′)

Splenial sulcus - *Sulcus splenialis* **#52** (Fig 1b:E′F′, Fig 3:A′)

Splenium of corpus callosum – *Splenium corporis callosi* **#93** (Fig 2:B′ Fig 3:A′)

Stria medularis thalami **#27** (Fig 1b:D′)

Substantia nigra **#46** (Fig 1b:E′, Fig 2:F′)

Suprasplenial gyrus - *Gyrus suprasplenialis* **#33** (Fig 1b:D′, E′, F′, Fig 3:B′)

Suprasylvian gyrus – *Gyrus suprasylvius* **#31** (Fig 1b:D′F′, Fig:2A′, Fig 3: C′, D′)

Suprasylvian sulcus – *Sulcus suprasylvius* **#42** (Fig 1b:D′, F′, Fig 2:A′)

Tectum of mesencephalon – *Tectum mesencephali* **#106** (Fig 3:A′)

Temporal lobe - *Lobus temporalis* #**35** (Fig 1b:D′)

Thalamus **#24** (Fig 1b:D′E′, Fig 2:C′, Fig 3:B′, C′)

Third ventricle – dorsal part – *Ventricularis tertius* **#84** (Fig 1b:D′, Fig 3:A′)

Third ventricle – ventral part – *Ventricularis tertius* **#83** (Fig 1b:D′, Fig 2:E′)

Trapezoid body – *Corpus trapezoideum* **#117** (Fig 3:B′)

Uvula **#100** (Fig 2:E′, F′, Fig 3:A′)

Ventral part of hippocampus **#86** (Fig 1b:D′, E′, Fig 2:E′F′, Fig 3:D′)

Vermis **#77** (Fig 1c:I′, Fig 2C′, D′)

Vestibular nucleus – *Nucleus vestibularis* **#62** (Fig 1c:G′, H′)

Supplementary Material

Refer to Web version on PubMed Central for supplementary material.

Abbreviations

FDA	Food and Drug Administration
MRI	magnetic resonance imaging
T1w	T1 weighted
T2w	T2 weighted
MPRAGE	magnetization-prepared rapid gradient echo
TSE	turbo spin echo
1.5T	1.5 tesla
3T	3 tesla
DLH	domestic long haired
TR	relaxation time
TI	inversion time
TE	excitation time
3D	three dimensional

BW	bandwidth
ms	milliseconds
Hz	hertz
mm	millimeters
mg/kg	milligram per kilogram
Fig	figure

References

Abramo F, Bo S, Canese MG, Poli A. Regional Distribution of Lesions in the Central-Nervous-System of Cats Infected with Feline Immunodeficiency Virus. Aids Res Hum Retrov. 1995; 11:1247–1253.

Alvarez-Linera J. 3T MRI: advances in brain imaging. European journal of radiology. 2008; 67:415–426. [PubMed: 18455895]

Aye MM, Izumo S, Inada S, Isashiki Y, Yamanaka H, Matsumuro K, Kawasaki Y, Sawashima Y, Fujiyama J, Arimura K, Osame M. Histopathological and ultrastructural features of feline hereditary cerebellar cortical atrophy: a novel animal model of human spinocerebellar degeneration. Acta neuropathologica. 1998; 96:379–387. [PubMed: 9797002]

Ba-Ssalamah A, Nobauer-Huhmann IM, Pinker K, Schibany N, Prokesch R, Mehrain S, Mlynarik V, Fog A, Heimberger K, Trattnig S. Effect of contrast dose and field strength in the magnetic resonance detection of brain metastases. Investigative radiology. 2003; 38:415–422. [PubMed: 12821855]

Baker HJ Jr, Lindsey JR, McKhann GM, Farrell DF. Neuronal GM1 gangliosidosis in a Siamese cat with beta-galactosidase deficiency. Science. 1971; 174:838–839. [PubMed: 5120520]

Bendinelli M, Pistello M, Lombardi S, Poli A, Garzelli C, Matteucci D, Ceccherininelli L, Malvaldi G, Tozzini F. Feline Immunodeficiency Virus - an Interesting Model for Aids Studies and an Important Cat Pathogen. Clin Microbiol Rev. 1995; 8:87–112. [PubMed: 7704896]

Berman, A. The thalamus and basal telencephalon of the cat: a cytoarchitectonic atlas with stereotaxic coordinates. Madison, WI: University of Wisconsin Press; 1982.

Berman, A.; Jones, EG. The brain stem of the cat: a cytoarchitectonic atlas with steriotaxic coordinates. Madison, WI: University of Wisconsin Press; 1968.

Bleier, R. the hypothalamus of the cat. Baltimore, MD: Johns Hopkins Press; 1961.

Bote RP, Blazquez-Llorca L, Fernandez-Gil MA, Alonso-Nanclares L, Munoz A, De Felipe J. Hippocampal sclerosis: histopathology substrate and magnetic resonance imaging. Seminars in ultrasound, CT, and MR. 2008; 29:2–14.

Bradbury AM, Cochran JN, McCurdy VJ, Johnson AK, Brunson BL, Gray-Edwards H, Leroy SG, Hwang M, Randle AN, Jackson LS, Morrison NE, Baek RC, Seyfried TN, Cheng SH, Cox NR, Baker HJ, Cachon-Gonzalez MB, Cox TM, Sena-Esteves M, Martin DR. Therapeutic response in feline sandhoff disease despite immunity to intracranial gene therapy. Mol Ther. 2013; 21:1306–1315. [PubMed: 23689599]

Bradbury AM, Morrison NE, Hwang M, Cox NR, Baker HJ, Martin DR. Neurodegenerative lysosomal storage disease in European Burmese cats with hexosaminidase beta-subunit deficiency. Molecular genetics and metabolism. 2009; 97:53–59. [PubMed: 19231264]

Bradbury AM, McCurdy VJ, Johnson AK, Gray-Edwards H, Brunson BL, Randle AN, Cox NR, Sena-Esteves M, Martin DR. Intracranial AAV Gene Therapy Extends the Life Span of GM2 Gangliosidosis Cats >4 Four-Fold with No Clinical Evidence of Vector Toxicity. Molecular Therapy. 2013; 21:226.

Bucher T, Colle MA, Wakeling E, Dubreil L, Fyfe J, Briot-Nivard D, Maquigneau M, Raoul S, Cherel Y, Astord S, Duque S, Marais T, Voit T, Moullier P, Barkats M, Joussemet B. scAAV9 Intracisternal Delivery Results in Efficient Gene Transfer to the Central Nervous System of a

Feline Model of Motor Neuron Disease. Human gene therapy. 2013; 24:670–682. [PubMed: 23799774]

Burditt LJ, Chotai K, Hirani S, Nugent PG, Winchester BG, Blakemore WF. Biochemical studies on a case of feline mannosidosis. The Biochemical journal. 1980; 189:467–473. [PubMed: 7213340]

Buxton, DF.; Compton, RW. The Canine Brain: Basic Atlas for an Auto-tutorial Approach to the Central Nervous System. 1986.

Candolfi M, Curtin JF, Nichols WS, Muhammad AG, King GD, Pluhar GE, McNiel EA, Ohlfest JR, Freese AB, Moore PF, Lerner J, Lowenstein PR, Castro MG. Intracranial glioblastoma models in preclinical neuro-oncology: neuropathological characterization and tumor progression. Journal of neuro-oncology. 2007; 85:133–148. [PubMed: 17874037]

Casal M, Haskins M. Large animal models and gene therapy. European journal of human genetics: EJHG. 2006; 14:266–272. [PubMed: 16333317]

Cork LC, Munnell JF, Lorenz MD. The pathology of feline GM2 gangliosidosis. The American journal of pathology. 1978; 90:723–734. [PubMed: 415617]

Cork LC, Munnell JF, Lorenz MD, Murphy JV, Baker HJ, Rattazzi MC. GM2 ganglioside lysosomal storage disease in cats with beta-hexosaminidase deficiency. Science. 1977; 196:1014–1017. [PubMed: 404709]

Costa LF, Paixao TA, Tsolis RM, Baumler AJ, Santos RL. Salmonellosis in cattle: advantages of being an experimental model. Research in veterinary science. 2012; 93:1–6. [PubMed: 22483382]

Duewell S, Wolff SD, Wen H, Balaban RS, Jezzard P. MR imaging contrast in human brain tissue: assessment and optimization at 4T. Radiology. 1996; 199:780–786. [PubMed: 8638005]

Dyce, KM.; Sack, WO.; Wensing, CJG. Textbook of Veterinary Anatomy. Elsevier Science Health Science Division; 2009.

Ellinwood NM, Vite CH, Haskins ME. Gene therapy for lysosomal storage diseases: the lessons and promise of animal models. The journal of gene medicine. 2004; 6:481–506. [PubMed: 15133760]

Eskandari R, Harris CA, McAllister JP 2nd . Reactive astrocytosis in feline neonatal hydrocephalus: acute, chronic, and shunt-induced changes. Child's nervous system: ChNS: official journal of the International Society for Pediatric Neurosurgery. 2011; 27:2067–2076.

Fatouros PP, Marmarou A. Use of magnetic resonance imaging for in vivo measurements of water content in human brain: method and normal values. Journal of neurosurgery. 1999; 90:109–115. [PubMed: 10413163]

Gitzelmann R, Bosshard NU, Superti-Furga A, Spycher MA, Briner J, Wiesmann U, Lutz H, Litschi B. Feline mucopolysaccharidosis VII due to beta-glucuronidase deficiency. Veterinary pathology. 1994; 31:435–443. [PubMed: 7941232]

Hasegawa D, Yamato O, Kobayashi M, Fujita M, Nakamura S, Takahashi K, Satoh H, Shoda T, Hayashi D, Yamasaki M, Maede Y, Arai T, Orima H. Clinical and molecular analysis of GM2 gangliosidosis in two apparent littermate kittens of the Japanese domestic cat. Journal of feline medicine and surgery. 2007; 9:232–237. [PubMed: 17198760]

Haskins ME, Jezyk PF, Desnick RJ, McDonough SK, Patterson DF. Alpha-L-iduronidase deficiency in a cat: a model of mucopolysaccharidosis I. Pediatric research. 1979; 13:1294–1297. [PubMed: 117422]

Haskins ME, Jezyk PF, Desnick RJ, Patterson DF. Animal model of human disease: Mucopolysaccharidosis VI Maroteaux-Lamy syndrome, Arylsulfatase B-deficient mucopolysaccharidosis in the Siamese cat. The American journal of pathology. 1981; 105:191–193. [PubMed: 6794375]

Hein WR, Griebel PJ. A road less travelled: large animal models in immunological research. Nature reviews Immunology. 2003; 3:79–84.

Hilton DL Jr, Einhaus SL, Meric AL 3rd, White RP, Schweitzer JB, Park MR, Robertson JT. Early assessment of neurologic deficits in the fluid percussion model of brain injury. Journal of neurotrauma. 1993; 10:121–133. [PubMed: 8411216]

International Committee of Veterinary Gross Anatomical Nomenclature I.C.V.G.A.N. Nomina Anatomica Veterinaria. 5. Hannover, Columbia MO, Ghent, Sapporo: 2005. (electronic format posted on the Web site of World Association of Veterinary Anatomists)

Johansen-Berg, H.; Behrens, TEJ. Diffusion MRI: From quantitative measurement to in-vivo neuroanatomy. Elsevier Science; 2009.

Johnson AK, McCurdy VJ, Bradbury AM, Gray-Edwards H, Randle AN, Huang M, Cox NR, Leroy SG, Sena-Esteves M, Martin DR. AAV Gene therapy Normalizes Disease Phenotype and Extends Lifespan >4 fold in Feline GM1 Gangliosidosis. Molecular Therapy. 2013; 21:226.

Khan T, Havey RM, Sayers ST, Patwardhan A, King WW. Animal models of spinal cord contusion injuries. Laboratory animal science. 1999; 49:161–172. [PubMed: 10331546]

Knake S, Triantafyllou C, Wald LL, Wiggins G, Kirk GP, Larsson PG, Stufflebeam SM, Foley MT, Shiraishi H, Dale AM, Halgren E, Grant PE. 3T phased array MRI improves the presurgical evaluation in focal epilepsies: a prospective study. Neurology. 2005; 65:1026–1031. [PubMed: 16217054]

Kroll RA, Pagel MA, Roman-Goldstein S, Barkovich AJ, D'Agostino AN, Neuwelt EA. White matter changes associated with feline GM2 gangliosidosis (Sandhoff disease): correlation of MR findings with pathologic and ultrastructural abnormalities. AJNR Am J Neuroradiol. 1995; 16:1219–1226. [PubMed: 7677013]

Kuhl CK, Textor J, Gieseke J, von Falkenhausen M, Gernert S, Urbach H, Schild HH. Acute and subacute ischemic stroke at high-field-strength (3.0-T) diffusion-weighted MR imaging: intraindividual comparative study. Radiology. 2005; 234:509–516. [PubMed: 15601894]

Lee SK, Kim DI, Kim SY, Kim DJ, Lee JE, Kim JH. Reperfusion cellular injury in an animal model of transient ischemia. AJNR Am J Neuroradiol. 2004; 25:1342–1347. [PubMed: 15466329]

Lowenthal AC, Cummings JF, Wenger DA, Thrall MA, Wood PA, de Lahunta A. Feline sphingolipidosis resembling Niemann-Pick disease type C. Acta neuropathologica. 1990; 81:189–197. [PubMed: 2127982]

Martin DR, Krum BK, Varadarajan GS, Hathcock TL, Smith BF, Baker HJ. An inversion of 25 base pairs causes feline GM2 gangliosidosis variant. Exp Neurol. 2004; 187:30–37. [PubMed: 15081585]

McCurdy, VJHlG-E.; Randle, Ashley N.; Bradbury, Allison M.; Johnson, Aime K.; Beadlescomb, Patricia M.; Morrison, Nancy; Hwang, Misako; Sena-Esteves, Miguel; Martin, Douglas R. Dramatic Phenotypic Improvement after Adeno-Associated Virus Gene Therapy in a Feline Model of Sandhoff Disease. Molecular Therapy. 2013; 21:15.

Meurens F, Summerfield A, Nauwynck H, Saif L, Gerdts V. The pig: a model for human infectious diseases. Trends in microbiology. 2012; 20:50–57. [PubMed: 22153753]

Mogicato G, Conchou F, Layssol-Lamour C, Raharison F, Sautet J. Normal feline brain: clinical anatomy using magnetic resonance imaging. Anatomia, histologia, embryologia. 2012; 41:87–95.

Ohshima T, Murray GJ, Swaim WD, Longenecker G, Quirk JM, Cardarelli CO, Sugimoto Y, Pastan I, Gottesman MM, Brady RO, Kulkarni AB. alpha-Galactosidase A deficient mice: a model of Fabry disease. Proc Natl Acad Sci U S A. 1997; 94:2540–2544. [PubMed: 9122231]

Phaneuf D, Wakamatsu N, Huang JQ, Borowski A, Peterson AC, Fortunato SR, Ritter G, Igdoura SA, Morales CR, Benoit G, Akerman BR, Leclerc D, Hanai N, Marth JD, Trasler JM, Gravel RA. Dramatically different phenotypes in mouse models of human Tay-Sachs and Sandhoff diseases. Human molecular genetics. 1996; 5:1–14. [PubMed: 8789434]

Podell M, Hadjiconstantinou M, Smith MA, Neff NH. Proton magnetic resonance imaging and spectroscopy identify metabolic changes in the striatum in the MPTP feline model of parkinsonism. Exp Neurol. 2003; 179:159–166. [PubMed: 12618122]

Podell M, March PA, Buck WR, Mathes LE. The feline model of neuroAIDS: understanding the progression towards AIDS dementia. J Psychopharmacol. 2000; 14:205–213. [PubMed: 11106298]

Sawaishi Y, Sasaki M, Yano T, Hirayama A, Akabane J, Takada G. A hippocampal lesion detected by high-field 3 tesla magnetic resonance imaging in a patient with temporal lobe epilepsy. The Tohoku journal of experimental medicine. 2005; 205:287–291. [PubMed: 15718821]

Schaller, O.; Constantinescu, GM. Illustrated Veterinary Anatomical Nomenclature: Enke Ferdinand. 2007.

Schneider JS, Yuwiler A, Markham CH. Production of a Parkinson-like syndrome in the cat with N-methyl-4-phenyl-1,2,3,6-tetrahydropyridine (MPTP): behavior, histology, and biochemistry. Exp Neurol. 1986; 91:293–307. [PubMed: 3484707]

Singer, M. The Brain of The Dog in Section. W.B. Saunders Company; 1962.

Smits M, Kovacs S, de Ridder D, Peeters RR, van Hecke P, Sunaert S. Lateralization of functional magnetic resonance imaging (fMRI) activation in the auditory pathway of patients with lateralized tinnitus. Neuroradiology. 2007; 49:669–679. [PubMed: 17404721]

Snider, R.; Niemer, WT. A Stereotaxic atlas of The Cat Brain. Chicago, IL: University of Chicago Press; 1970.

Strong AJ, Anderson PJ, Watts HR, Virley DJ, Lloyd A, Irving EA, Nagafuji T, Ninomiya M, Nakamura H, Dunn AK, Graf R. Peri-infarct depolarizations lead to loss of perfusion in ischaemic gyrencephalic cerebral cortex. Brain: a journal of neurology. 2007; 130:995–1008. [PubMed: 17438018]

Suzuki K. Genetic galactosylceramidase deficiency (globoid cell leukodystrophy, Krabbe disease) in different mammalian species. Neurochemical pathology. 1985; 3:53–68. [PubMed: 3895053]

Takahashi M, Uematsu H, Hatabu H. MR imaging at high magnetic fields. European journal of radiology. 2003; 46:45–52. [PubMed: 12648801]

Toyota S, Graf R, Valentino M, Yoshimine T, Heiss WD. Malignant infarction in cats after prolonged middle cerebral artery occlusion: glutamate elevation related to decrease of cerebral perfusion pressure. Stroke; a journal of cerebral circulation. 2002; 33:1383–1391.

Vinogradov E, Degenhardt A, Smith D, Marquis R, Vartanian TK, Kinkel P, Maier SE, Hackney DB, Lenkinski RE. High-resolution anatomic, diffusion tensor, and magnetization transfer magnetic resonance imaging of the optic chiasm at 3T. Journal of magnetic resonance imaging: JMRI. 2005; 22:302–306. [PubMed: 16028247]

Vite CH, Magnitsky S, Aleman D, O'Donnell P, Cullen K, Ding W, Pickup S, Wolfe JH, Poptani H. Apparent diffusion coefficient reveals gray and white matter disease, and T2 mapping detects white matter disease in the brain in feline alpha-mannosidosis. AJNR Am J Neuroradiol. 2008; 29:308–313. [PubMed: 17974615]

Vite CH, McGowan JC, Braund KG, Drobatz KJ, Glickson JD, Wolfe JH, Haskins ME. Histopathology, electrodiagnostic testing, and magnetic resonance imaging show significant peripheral and central nervous system myelin abnormalities in the cat model of alpha-mannosidosis. Journal of neuropathology and experimental neurology. 2001; 60:817–828. [PubMed: 11487056]

Vite CH, McGowan JC, Niogi SN, Passini MA, Drobatz KJ, Haskins ME, Wolfe JH. Effective gene therapy for an inherited CNS disease in a large animal model. Ann Neurol. 2005; 57:355–364. [PubMed: 15732095]

Vite CH, Passini MA, Haskins ME, Wolfe JH. Adeno-associated virus vector-mediated transduction in the cat brain. Gene therapy. 2003; 10:1874–1881. [PubMed: 14502216]

Vite CH, Wang P, Patel RT, Walton RM, Walkley SU, Sellers RS, Ellinwood NM, Cheng AS, White JT, O'Neill CA, Haskins M. Biodistribution and pharmacodynamicsof recombinant human alpha-L-iduronidase (rhIDU) in mucopolysaccharidosis type I-affected cats following multiple intrathecal administrations. Molecular genetics and metabolism. 2011; 103:268–274. [PubMed: 21482164]

Wattjes MP, Harzheim M, Kuhl CK, Gieseke J, Schmidt S, Klotz L, Klockgether T, Schild HH, Lutterbey GG. Does high-field MR imaging have an influence on the classification of patients with clinically isolated syndromes according to current diagnostic mr imaging criteria for multiple sclerosis? AJNR Am J Neuroradiol. 2006; 27:1794–1798. [PubMed: 16971638]

Woermann FG, Vollmar C. Clinical MRI in children and adults with focal epilepsy: a critical review. Epilepsy & behavior: E&B. 2009; 15:40–49.

Highlights

- Highest resolution cat MRI anatomy is provided with 119 structures in three planes.
- The constituents of the visual, auditory and motor pathways are clearly visualized.
- Previously unresolvable cerebellar and vestibular nuclei, are clearly identified.
- The detail is sufficient to illustrate cerebral vasculature.
- These findings are applicable to human diseases modeled in the cat.

Figure1a

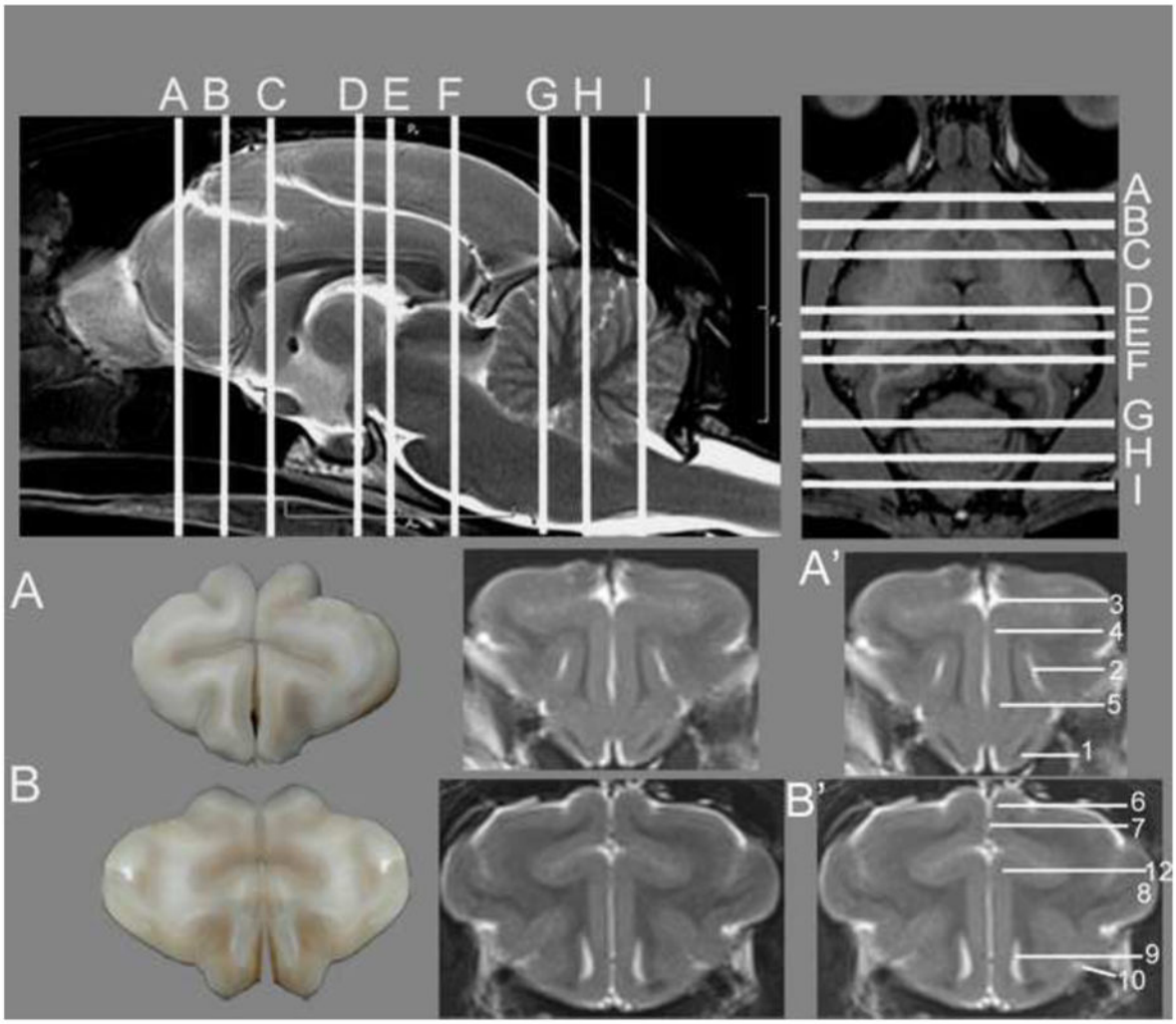

Figure1b

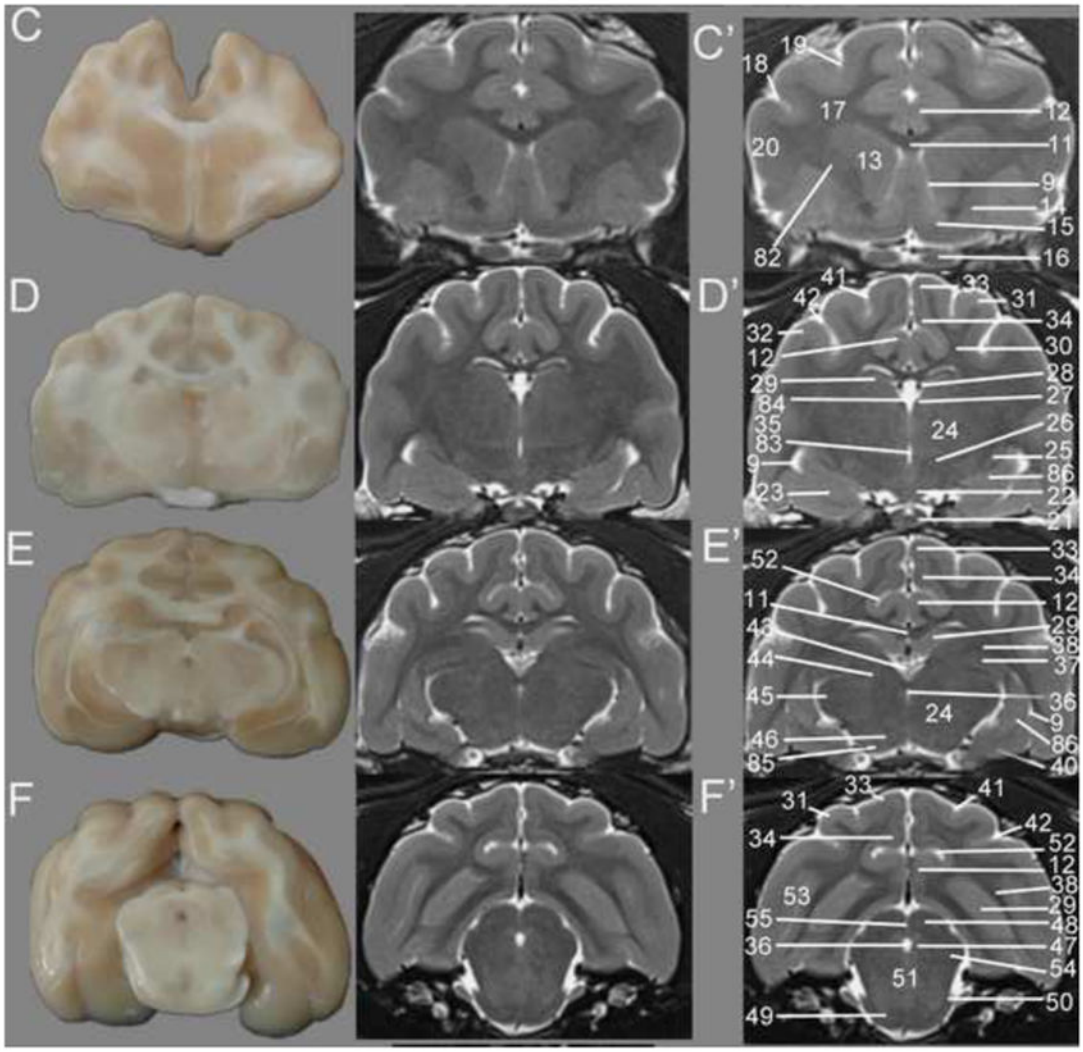

Figure1c

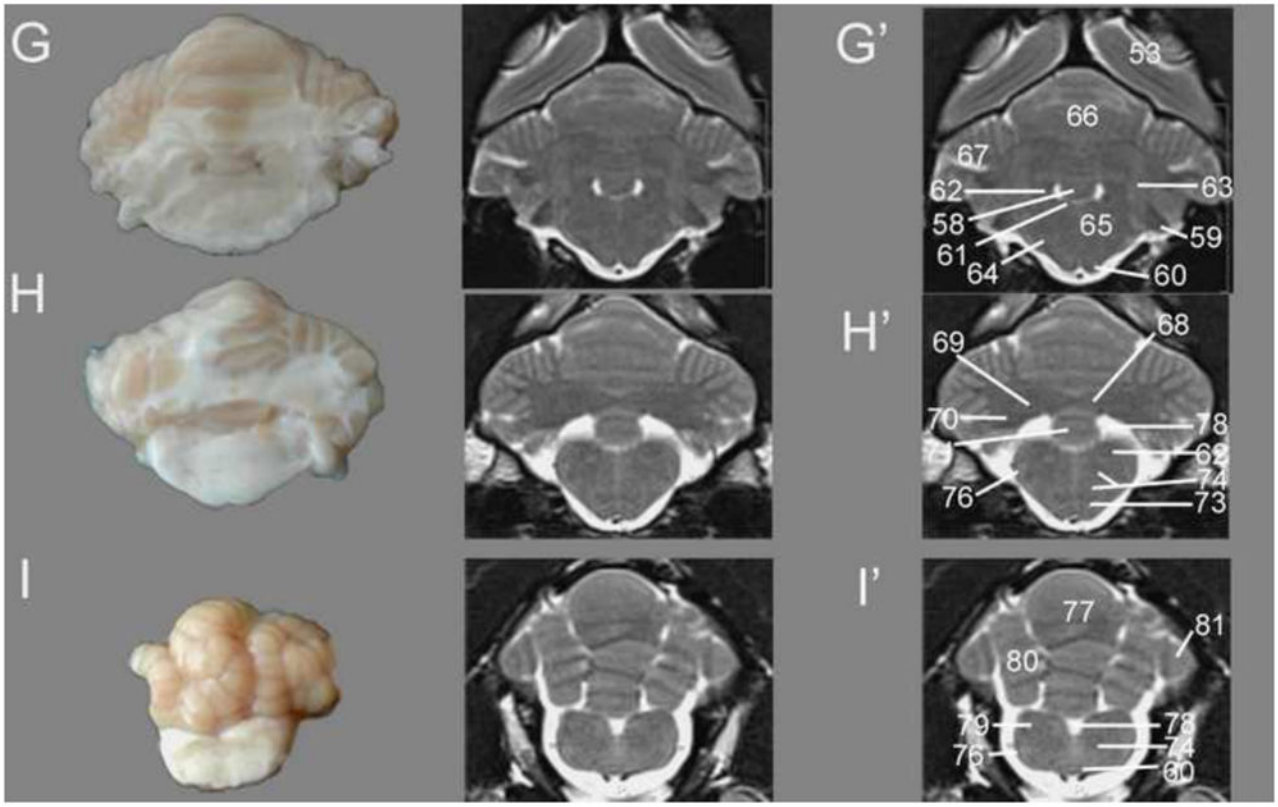

Figure 1.

Figure 1a. Transverse T2w images of the cat brain. Top: sagittal and dorsal localizer denoting location of transverse sections. These slices correlate with Figures 1.a, 1.b and 1.c. Gross section of the cat brain (left – A and B) correlating with the unlabeled (middle) and labeled MRI images (right – A′ and B′). A – most rostral aspect of the frontal cortex, B – caudal portion of frontal cortex. Identified anatomical structures are listed in the image key and numbering is consistent throughout images.

Figure 1b. Transverse T2w images of the cat brain. Sagittal and dorsal localizer denoting locations of transverse sections are located in Figure 1.a. Gross section of the cat brain (left A–F) correlating with the unlabeled (middle) and labeled MRI images (right – C′-F′). C – striatum, D – rostral thalamus, E -caudal thalamus, F- midbrain and occipital cortex. Identified anatomical structures are listed in the image key and numbering is consistent throughout images.

Figure 1c. Transverse T2w images of the cat brain. Sagittal and dorsal localizer denoting locations of transverse sections are located in Figure 1.a. Gross section of the cat brain (left – G–I) correlating with the unlabeled (middle) and labeled MRI images (right – G′-I′). G – rostral cerebellum, H - middle cerebellum, I – caudal cerebellum. Identified anatomical structures are listed in the image key and numbering is consistent throughout images.

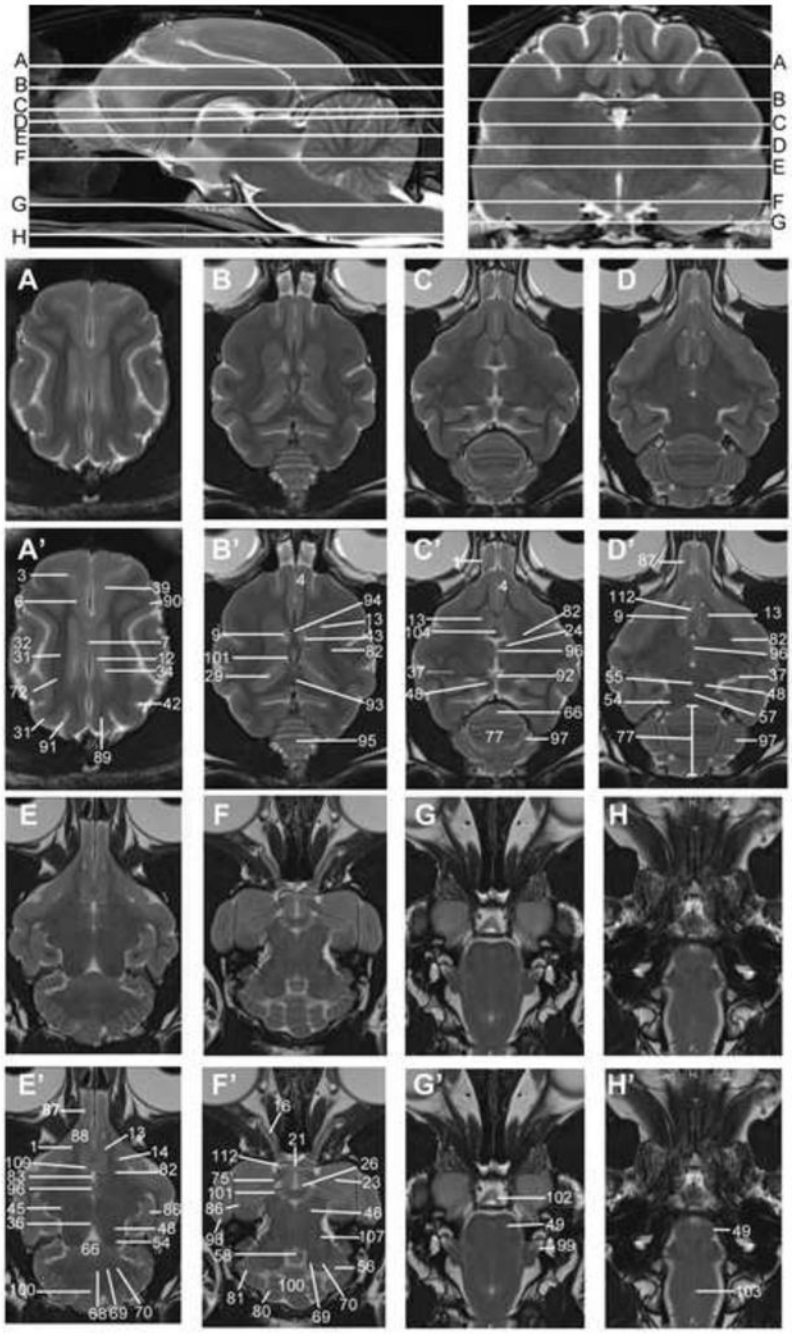

Figure 2.

Dorsal T2w images of the cat brain. Top: sagittal and transverse localizer denoting location of dorsal sections. Sections begin at the dorsal aspect of the brain (A) and extend ventrally to the caudal brainstem and spinal cord (H). Unlabeled images are located above the labeled MRI images (denoted by prime symbol). Identified anatomical structures are listed in the image key and numbering is consistent throughout images.

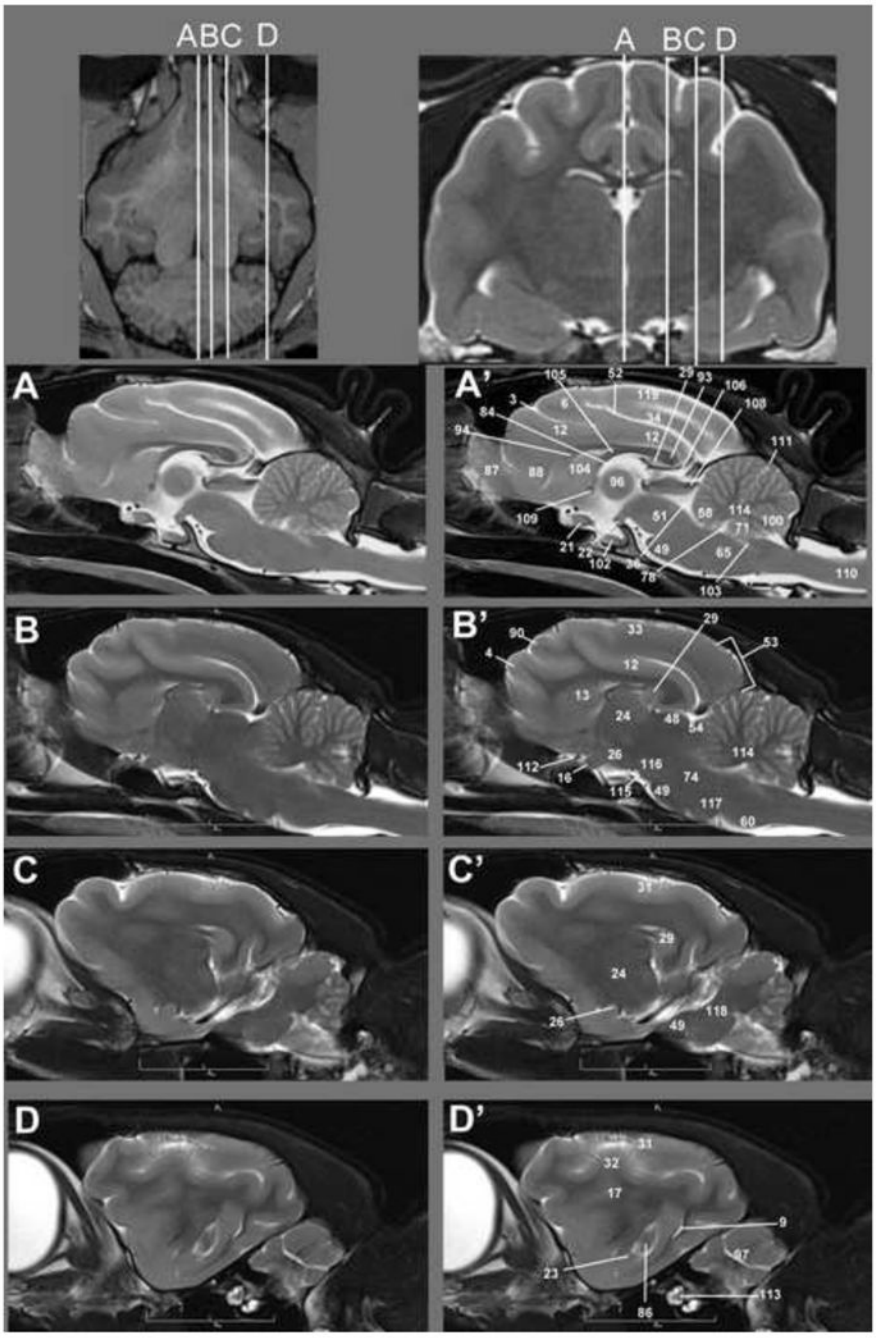

Figure 3.

Sagittal T2w images of the cat brain. Top: Dorsal and transverse localizer denoting location of dorsal sections. Sections begin on midline (A) and extend out laterally through the hemisphere (D) Unlabeled images are located left (A–D) of the labeled MRI images (right A ′-D′). Identified anatomical structures are listed in the image key and numbering is consistent throughout images.

3D Neuroimaging. 3D T1w MPRAGE MRI. Sagittal, transverse and dorsal planes are available to be visualized simultaneously. Crosshairs denotes area of brain examined and its location in all three views.